JCB Article

deep-orange and *carnation* define distinct stages in late endosomal biogenesis in *Drosophila* melanogaster

V. Sriram,[1] K.S. Krishnan,[2] and Satyajit Mayor[1]

[1]National Centre for Biological Sciences, Tata Institute for Fundamental Research, Bangalore 560 065, India
[2]Department of Biological Sciences, Tata Institute for Fundamental Research, Mumbai 400 005, India

Endosomal degradation is severely impaired in primary hemocytes from larvae of eye color mutants of *Drosophila*. Using high resolution imaging and immunofluorescence microscopy in these cells, products of eye color genes, *deep-orange (dor)* and *carnation (car)*, are localized to large multivesicular Rab7-positive late endosomes containing Golgi-derived enzymes. These structures mature into small sized Dor-negative, Car-positive structures, which subsequently fuse to form tubular lysosomes. Defective endosomal degradation in mutant alleles of *dor* results from a failure of Golgi-derived vesicles to fuse with morphologically arrested Rab7-positive large sized endosomes, which are, however, normally acidified and mature with wild-type kinetics. This locates the site of Dor function to fusion of Golgi-derived vesicles with the large Rab7-positive endocytic compartments. In contrast, endosomal degradation is not considerably affected in *car*^{1} mutant; fusion of Golgi-derived vesicles and maturation of large sized endosomes is normal. However, removal of Dor from small sized Car-positive endosomes is slowed, and subsequent fusion with tubular lysosomes is abolished. Overexpression of Dor in *car*^{1} mutant aggravates this defect, implicating Car in the removal of Dor from endosomes. This suggests that, in addition to an independent role in fusion with tubular lysosomes, the Sec1p homologue, Car, regulates Dor function.

Introduction

Late endosomes and lysosomes are main degradative compartments within the endosomal system in metazoans, identified by their characteristic multivesicular morphology and absence of recycling receptors (Storrie and Desjardins, 1996; Luzio et al., 2000; Mullins and Bonifacino, 2001). Late endosomes are extremely dynamic organelles undergoing large scale morphological transformations (Gruenberg and Maxfield, 1995). They are capable of fusion with maturing early endosomes or carrier vesicles (Gruenberg et al., 1989), homotypic fusion to affect multivesicularization (Antonin et al., 2000), and finally heterotypic fusion to transfer contents to lysosomes (Luzio et al., 2000). In addition to endocytosed contents from early endosomes, multivesicular late endosomes also fuse with vesicles derived from the trans-Golgi network (Griffiths et al., 1988; Glickman and Kornfeld, 1993; Mullins and Bonifacino, 2001; Piper and Luzio, 2001).

This system of organelles is critical for a variety of processes in metazoans: cessation of mitogenic signaling, turnover of normal cellular proteins, disposal of abnormal proteins, antigen processing, and release of endocytosed nutrients in endolysosomes (Mullins and Bonifacino, 2001). Important clues to understanding mechanisms of development have come from analyses of animals carrying mutations in genes proposed to be involved in lysosomal delivery and degradation. Lysosomal function decides the range of action of morphogens during development by modulating the duration of intracellular signaling of ligand-bound signaling receptors (Babst et al., 2000; Dubois et al., 2001).

Genetic analysis has provided an understanding of the role of molecular players involved in secretory traffic and vacuole biogenesis in *Saccharomyces cerevisiae* (Horazdovsky et al., 1995; Wendland et al., 1998). Analyses of vacuolar protein sorting has led to the identification of over 50 genes involved in vacuolar biogenesis in yeast (Bryant and Stevens, 1998). These genes, referred to as vacuolar protein sorting (*vps*)* or *vam* genes (Wickner, 2002) are subdivided into six classes (A–F) based on their vacuolar phenotypes (Banta et al., 1988;

The online version of this article includes supplemental material.

Address correspondence to Satyajit Mayor, National Centre for Biological Sciences, Tata Institute for Fundamental Research (TIFR), UAS-GKVK Campus, Bellary Rd., Bangalore 560 065, India. Tel.: 91-80-3636420, ext. 4260 Fax: 91-80-3636662. E-mail: mayor@ncbs.res.in

*Abbreviations used in this paper: *car, carnation*; DAB, diaminobenzidine; *dor*, *deep-orange*; dSR, *Drosophila* scavenger receptor; F-Dex, FITC-dextran; Fl-mBSA, fluorescently conjugated mBSA; LR-Dex, lissamine rhodamine–labeled dextran; mBSA, maleylated BSA; MVB, multivesicular body; *vps*, *vacuolar protein sorting*; Y*dor*$^{+}$, Dp(Y:1)1E.

Key words: lysosome; endosome; maturation; cell culture; cathepsin L

Robinson et al., 1988). Development of assays for vesicle fusion in vitro has also provided insight into the biochemical functions of these genes (Wickner, 2002). Since the yeast vacuole is proposed to be functionally analogous to lysosomes in metazoans (Lloyd et al., 1998; Odorizzi et al., 1998; Dell'Angelica et al., 2000), homologues of these genes are likely to be used in constructing endolysosomes in metazoans.

To analyze the role of genes involved in endolysosomal biogenesis in a metazoan, we have been able to reproducibly derive primary cultures of hemocytes from *Drosophila* melanogaster. We have shown (Guha et al., 2003) that larval hemocytes from animals mutant at the *shibire* locus exhibit a temperature-sensitive, reversible inhibition of receptor-mediated endocytosis, faithfully reproducing temperature-sensitive paralysis phenotype observed in *shi* flies (Krishnan et al., 1996).

Here we have examined the perturbation of late endosomal trafficking and degradation in two mutants, *deep-orange (dor)* and *carnation (car)*. These genes are part of the "granule group" of eye color genes in *Drosophila* (Lloyd et al., 1998; Odorizzi et al., 1998; Spritz, 1999), which reduce both red and brown eye pigments and encode fly homologues of yeast genes, *VPS18* and *VPS33*, respectively (Mullins and Bonifacino, 2001). 85 mutations affecting eye color have been isolated, and a subset is proposed to be involved in pigment granule biogenesis, an organelle whose biogenesis may resemble that of lysosomes (Lloyd et al., 1998; Dell'Angelica et al., 2000). The availability of a cell culture system provides an opportunity wherein mutations in genes involved in lysosomal biogenesis that give rise to phenotypes in the animal may be analyzed at the cellular level at high resolution.

VPS18 and *VPS33* are part of class C *vps* genes, which also includes *VPS11* and *VPS16* and whose products assemble as a complex called the class C complex (Sato et al., 2000; Wurmser et al., 2000). The VPS18p homologue, Dor, associates with endosomal membranes in *Drosophila* cells (Sevrioukov et al., 1999). Clones of a null mutant, dor^{8} in the compound eye of *Drosophila* are pigmentation deficient, and consistent with an effect on lysosomal degradation, endocytosed HRP-Boss ligand accumulates intracellularly in aberrant multivesicular structures (Sevrioukov et al., 1999). The role of Dor in lysosomal function is further suggested by the lack of degradation of overexpressed Wingless-HRP in dor^{8} embryos (Dubois et al., 2001). However, the reason for this defect in degradation in terms of the pathways perturbed in a metazoan system is yet unknown. The VPS33p homologue, Car, associates with Dor in vitro (Sevrioukov et al., 1999); *car* genetically interacts with *dor* (Lindsley and Zimm, 1992). These observations implicate Dor and Car in biogenesis of endolysosomes in metazoa.

To study biogenesis of endolysosomes and role(s) of Dor and Car in this process, we have followed the endocytic fate of molecules internalized by endogenously expressed anionic ligand binding receptors resembling *Drosophila* scavenger receptors (dSRs; unpublished data) using fluorescently labeled protein ligands for dSR together with probes for fluid phase endocytosis (e.g., fluorescently labeled dextrans) in hemocytes. We show that in Rab7-positive endosomal system, multivesicular late endosomes contain both Dor and Car and mature into small dense Dor-negative but Car-positive endosomes. These endosomes eventually fuse with tubular lysosomes. We have then addressed the role of Dor and Car in biogenesis of these different types of Rab7-positive endosomal compartments using a combination of high resolution fluorescence microscopy and EM. We provide evidence that Dor is required for fusion of Golgi-derived vesicles rich in hydrolytic enzymes with large multivesicular endocytic compartments. On the other hand, Car appears to function in removal of Dor from maturation-competent Rab7-positive late endosomes. It is also involved in fusion of small dense Dor-negative, Car-positive organelles with tubular lysosomes, providing evidence for a function independent of Dor.

Results

Morphological characterization of the endocytic pathway in larval hemocytes from wild-type animals

In a recent study (Guha et al., 2003), we have shown that fluorescently conjugated maleylated BSA (Fl-mBSA) binds specifically to endogenously expressed dSR at the cell surface of hemocytes (Fig. 1 A) and is then internalized via a dynamin (*shibire)*-dependent pathway into early sorting endosomes marked by the small GTPase Rab5. On the other hand, majority of the fluid phase is internalized via a *shibire*-independent pathway into distinct Rab5-negative endosomes. Similar to a recently described pathway in mammalian cells (Sabharanjak et al., 2002), both these populations of endosomes were not labeled by the late endosomal marker Rab7; subsequent incubation in the absence of fluorescently labeled probes for 5 min (a chase of 5 min) results in dSR ligand and fluid phase probes becoming extensively colocalized as observed in fixed cells (Fig. 1 B).

In live hemocytes, upon incubation with fluorescently labeled probes for 5 min (5-min pulse) the majority of Fl-mBSA and lissamine rhodamine–labeled dextran (LR-Dex) are colocalized in large endosomal compartments often near the center of the cell (Fig. 1 C, open arrowheads). Lumenal connectivity of Fl-mBSA and a fluid phase probe in these large (1–2 μm) endosomes at 5 min was confirmed by HRP-mediated quenching (Mayor et al., 1998) of Fl-mBSA fluorescence by diaminobenzidine (DAB) radicals generated from HRP cointernalized via the fluid phase (unpublished data). In some endosomes, dSR ligands label only the limiting membrane, whereas the fluid tracer labels the lumen of the organelle (Fig. 1 C, open arrowheads and top inset). Ultrastructure analyses by EM of endosomes labeled by a 10-min pulse of fluid phase HRP (Fig. 1 G i) revealed a multivesicular morphology; HRP labels the lumen of the compartment and is excluded from luminal vesicles (Fig. 1 G ii, arrows). These criteria establish that endosomes accessed by a 5-min pulse of the two probes are similar to late endosomes (multivesicular bodies [MVBs]) observed in mammalian cells (Piper and Luzio, 2001). To confirm the identity of the 5-min-labeled organelles as late endosomes, we used antibodies generated against mammalian Rab7 (Chavrier et al., 1990), which recognizes *Drosophila* Rab7 expressed in these cells (Fig. S1, available at http://www.jcb.org/cgi/content/full/jcb.20010166/DC1); mAb against lysobisphosphatidic acid (anti-LBPA, 6C4; Kobayashi et al., 1998) also labels the same

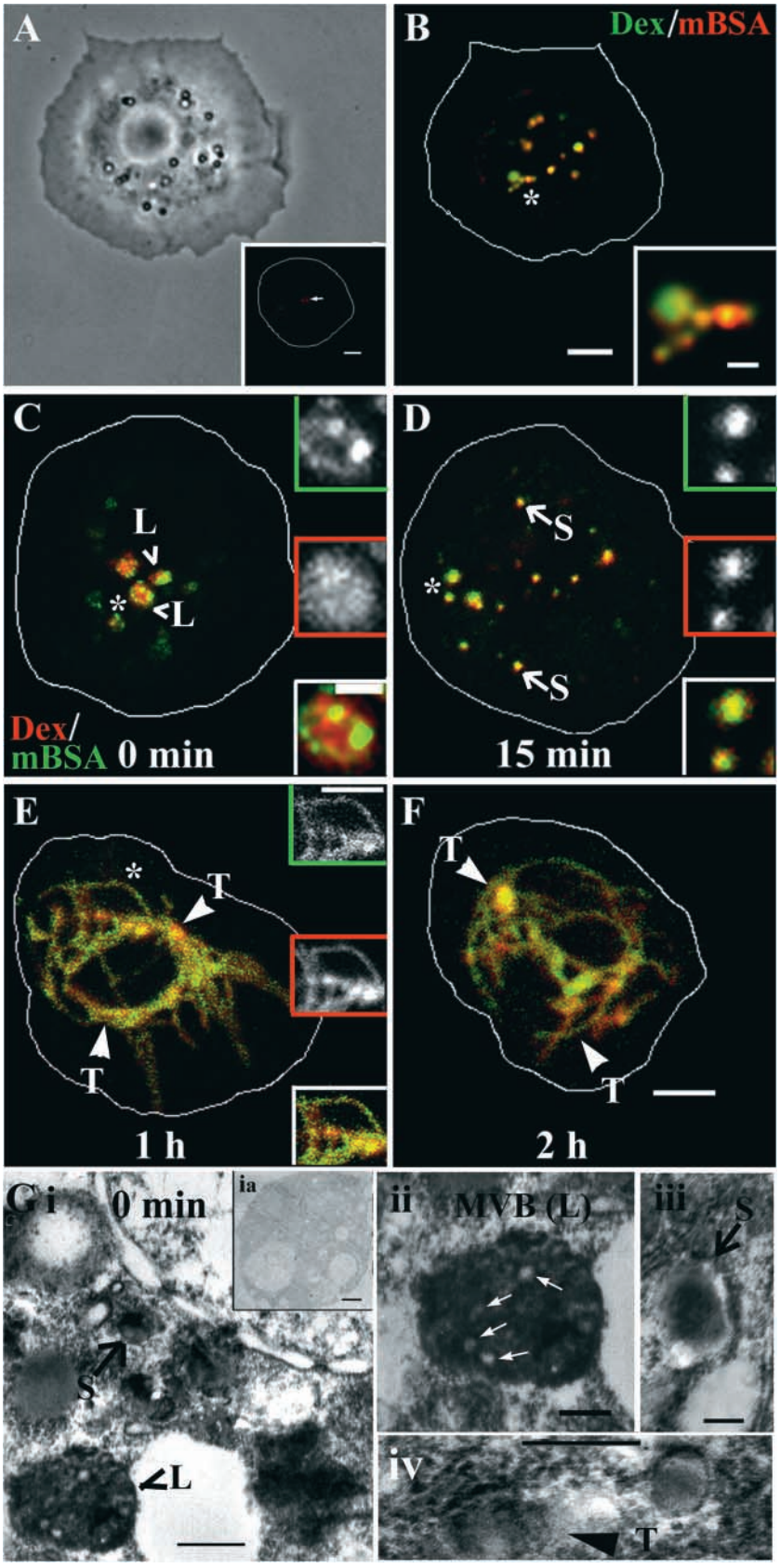

Figure 1. **Morphological characterization of the endocytic pathway in *Drosophila* larval hemocytes.** (A and B) Phase–contrast (A) and fluorescence (B) images of larval hemocytes incubated with Cy3-mBSA (mBSA, 800 ng/ml; red in B) and F-Dex (Dex, 1 mg/ml; green in B) for 5 min and fixed, obtained using a wide field microscope, show that Dex and mBSA are completely colocalized in endosomes (B, inset). Uptake of Cy3-mBSA is completely competed by inclusion of unlabeled mBSA (A, inset). (C–F) Confocal images of live larval hemocytes incubated with LR-Dex (Dex, red) and A_{488}-mBSA (mBSA, green) for 5 min were obtained either immediately (C) or after a chase period of 15 min (D), 1 h (E), or 2 h (F) without the probes. Insets in B–E show magnified view of areas marked by an asterisk. (C) Endosomes labeled by the 5-min pulse are large (1–2 μm; L, open arrowheads) in size in which Dex labels the lumen of the endosome (middle inset); occasionally intraendosomal membrane staining of mBSA (top inset) can also be seen (bottom inset). (D) In a 15-min chase, Dex (middle inset) and mBSA (top inset) label smaller compartments (0.5–1 μm; S, arrows) where the probes are completely colocalized (bottom inset). (E and F) After a 1- (E) or 2-h (F) chase, both probes remain colocalized, appearing predominantly in tubular-vesicular (T, arrowheads) endosomal compartments (Dex, middle; mBSA, top inset). Bars: (shown in B corresponds to A–F) 5 μm; 1 μm (B–D, insets); 5 μm (A and E, insets). (G) EM of hemocyte incubated with fluid phase HRP for 10 min in the presence of mannan (500 μg/ml) to prevent mannose receptor–mediated uptake of HRP. Cells were fixed and processed for EM either immediately (i–iii) or after a 50-min chase (iv). At 10 min (i and ii), HRP labels MVBs (open arrowhead) and small dense endosomes (iii, arrow). No significant electron-dense structures could be identified in cells that were processed without HRP (unpublished data) or DAB (inset, ia). At higher magnification, the multivesicular nature of the endosome (ii, small arrows, intraendosomal vesicles) and the small densely labeled compartments (iii) are more apparent. Small electron-dense compartments are also visualized by HRP product when 10-min pulse is chased for 50 min (iv, arrowhead) consistent with a fixation-induced fragmentation of tubular vesicular endosomes observed at this time (E). Bars: (G i) 500 nm; (G ia) 1 μm; (G ii–iv) 200 nm.

endosomes (Fig. S1). In addition, endosomes accessed by a 5-min pulse of Fl-mBSA are also labeled by antiserum to Hrs and Hook proteins (Fig. S2, available at http://www.jcb.org/cgi/content/full/jcb.20010166/DC1), markers of late endosomal compartments identified previously in garland cells in *Drosophila* (Kramer and Phistry, 1996; Lloyd et al., 2002).

After a 5-min pulse, increasing chase times (Fig. 1, D–F) result in major morphological changes in endosomal com-

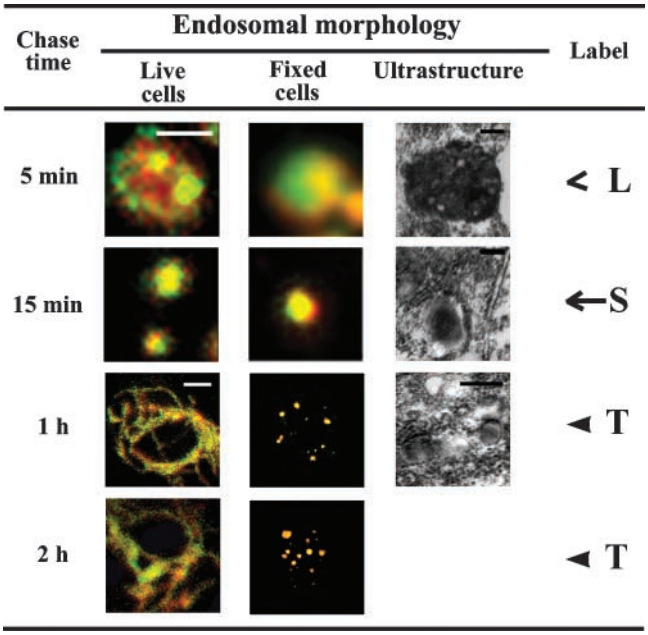

Figure 2. **Morphology of endosomes in live and fixed cells.** Hemocytes were either imaged live or after fixation following a pulse and chase protocol with Dex (red, live cells; green, fixed cells; 5-min pulse) and mBSA (green, live cells; red, fixed cells; 5-min pulse), or HRP (Ultrastructure; 10-min pulse) at the indicated chase times. Morphology of the endosomes was visualized by confocal (live cells), wide field (fixed), or electron microscopy (HRP). Bars: (5 min and 15 min; live and fixed cells) 1 μm; (1 h and 2 h; live and fixed cells) 5 μm; (Ultrastructure) 200 nm. The labels L, S, and T identify the large sized, small sized, and tubular-vesicular endosomes in all of the figures in this study.

partments accessed by Fl-mBSA and LR-Dex, clearly distinguishing them from MVBs observed at 5 min. After a 15-min chase period, endosomes appear smaller (0.5–1.0 μm) and show complete colocalization of Fl-mBSA and fluid tracer within the endosome (Fig. 1 D, arrows and inset). EM analysis confirms the formation of small HRP-filled electron-dense structures (Fig. 1 G iii). After a 1-h chase, endosomal morphology is tubular-vesicular (Fig. 1 E), and this persists for 2 (Fig. 1 F) to 4 h (data not depicted). This tubular morphology is sensitive to osmotic stress (unpublished data), analogous to tubular lysosomes observed in mammalian bone marrow–derived macrophages labeled with the fluid tracer lucifer yellow (Knapp and Swanson, 1990) and conventional fixing protocols. Tubules are not observed by fluorescence (Fig. 3 C) and EM analyses (Fig. 1 G iv) of fixed samples. Comparison of the morphology of endosomes as a function of chase times in live cells versus those obtained in fixed cells is shown in Fig. 2.

To address the identity of the morphologically distinct compartments accessed by the endocytic probes at different chase times, we first asked whether they are marked by Rab7. The fraction of FITC-dextran (F-Dex)–containing endosomes (at different chase times after a 15-min pulse of the endocytic probe) labeled by Rab7 was quantified as described (see Materials and methods). Quantitative analysis shows that majority of F-Dex–containing endosomes at chase times described above are positive for Rab7 (Fig. 3).

Together with observations made in a separate study (Guha et al., 2003), these observations show that endocytosed probes in larval hemocytes are first delivered to a collection of Rab7-negative early endosomes followed by

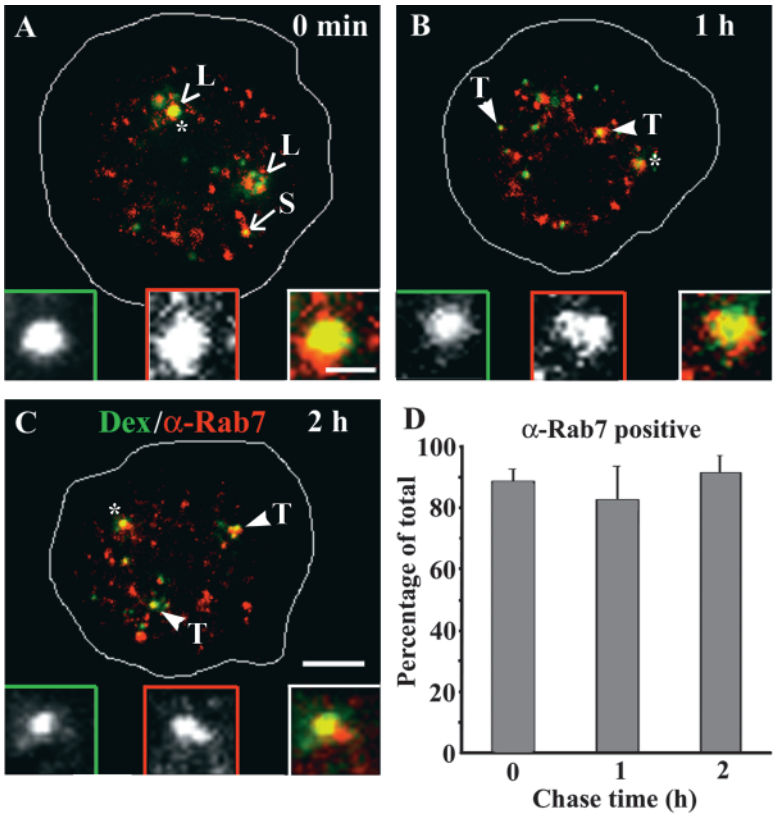

Figure 3. **Rab7 labels endolysosomes in larval hemocytes.** (A–C) Hemocytes incubated with F-Dex for 15 min were fixed either immediately (A) or, after a 1- (B) or 2-h (C) chase period in the absence of endocytic probe, immunostained for Rab7 and imaged on a confocal microscope. Images show that Rab7 (red; middle insets) labels different stages of the endosomal system accessed by endocytosed F-Dex (green, left insets) after indicated chase times. Insets show a magnified view of areas marked by an asterisk. (D) Histogram shows the percentage of F-Dex–containing endosomes per cell colocalized with immunolocalized Rab7. The results shown represent the mean ± SEM obtained from two experiments. Bars: (shown in C corresponds to A–C) 5 μm; (insets) 1 μm.

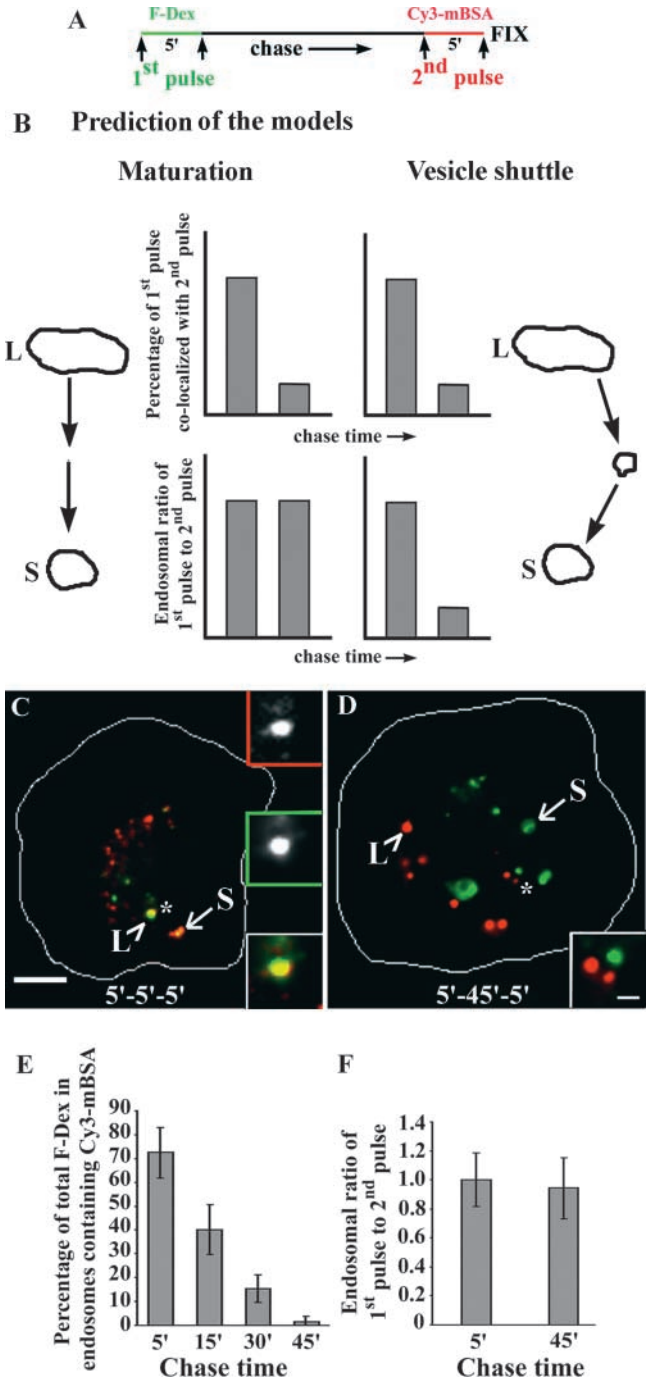

Figure 4. **Multivesicular late endosomes mature into small dense organelles in hemocytes from wild-type animals.** (A and B) Hemocytes derived from wild-type larvae were incubated according to the pulse–chase–pulse protocol outlined in A with F-Dex (green) as first pulse and Cy3-mBSA (red) as second pulse, fixed, and imaged on wide-field microscope. (B) Outline of the predictions of maturation (left) and vesicle shuttle (right) models. This is in terms of kinetics of loss of fusion accessibility (top) and the change in ratio of amount of the first pulse to amount of colocalized second pulse in an endosome as a function of chase time (bottom). (C–F) Comparison of a 5- (C; F-Dex, middle; mBSA, top inset) with a 45-min chase time (D; F-Dex, arrow; mBSA, open arrowhead) between the two probes shows that the percentage of endosomes containing first probe and accessible to second probe reduces with increasing chase times. Insets in C and D show magnified views of areas marked by an asterisk. Histograms show kinetics of loss of fusion accessibility (E) and the relative ratio of amount of first pulse remaining in an endosome to amount of colocalized second pulse in the same endosome as a function of chase time (F). The data in E and F represent the median ± SD derived from two experiments. Bars: (shown in C corresponds to C and D) 5 μm; (insets) 1 μm.

subsequent delivery to Rab7-positive multivesicular late endosomes. After a chase of 1 h (or 2 h), probes are visualized in Rab7-positive lysosomal network that is a tubular-vesicular system in live cells (Fig. 2). Although, these endosomal stages are persistently labeled by Rab7, they exhibit a characteristic dynamic of multiple molecular players as detailed below (see Fig. 11).

Multivesicular large sized endosomes in wild-type cells mature into fusion-inaccessible small dense organelles

We next probed the process by which endosomal cargo is trafficked between large sized endosomes and small dense endosomes formed in wild-type cells. There are mainly two ways this trafficking can happen: (1) via transformation of the large sized endosomes into the small dense endosomes (maturation process) or (2) vesicle budding from large sized endosomes, fusing with small dense endosomes (vesicle shuttle) (Fig. 4 B). These processes have distinct predictions for the mixing of endosomal contents between two temporally separated endocytic probe pulses (Fig. 4 A). Measuring the ratio of the amount of the two probes in colocalized endosomal compartments at different chase times provides a method of distinguishing between the vesicle shuttle and maturation models of endosomal trafficking between two types of organelles (Stoorvogel et al., 1991; Dunn and Maxfield, 1992).

Using F-Dex as the first pulse (Fig. 4, A, C, and D, green) and Cy3-mBSA as the second pulse (Fig. 4, A, C, and D, red), we monitored the extent of fusion accessibility of the first pulse–containing endosomes to the second pulse with increasing chase times between the two pulses (Fig. 4, A, C, and D). As a control, we ensured that Cy3-mBSA and F-Dex label the same late endocytic compartments with comparable kinetics when pulsed in together (Fig. 1). The endosomes containing first pulse are completely accessible to the second pulse at short chase times (Fig. 4 C, open arrowhead and arrow). A longer chase of first pulse–containing endosomes results in morphological transformation to small dense endosomes (Fig. 1) becoming fusion inaccessible (Fig. 4 D, arrow); the first pulse loses fusion accessibility with a half time of ~12 min (Fig. 4 E). After a chase time of 5 min, fusion accessibility of the Rab7-positive large endosomes (Figs. 1 and 3) is corroborated by complete quenching (~80 ± 10%) of first pulse of Cy3-mBSA fluorescence by DAB-mediated radicals generated from a second pulse of HRP. Consistent with the loss of colocalization, after a chase of 45 min Cy3-mBSA fluorescence (first pulse) is protected (only ~40 ± 20% is quenched) from HRP second pulse.

The mere loss of fusion accessibility does not discriminate between the two models. If a vesicle shuttle mechanism is involved in traffic between large endosomes and small compartments (or if small compartments represent vesicles in transit between two stages of the endocytic pathway), with increasing chase times (Fig. 4 B) the endosomes accessible to the second pulse will gradually lose the first pulse to the next

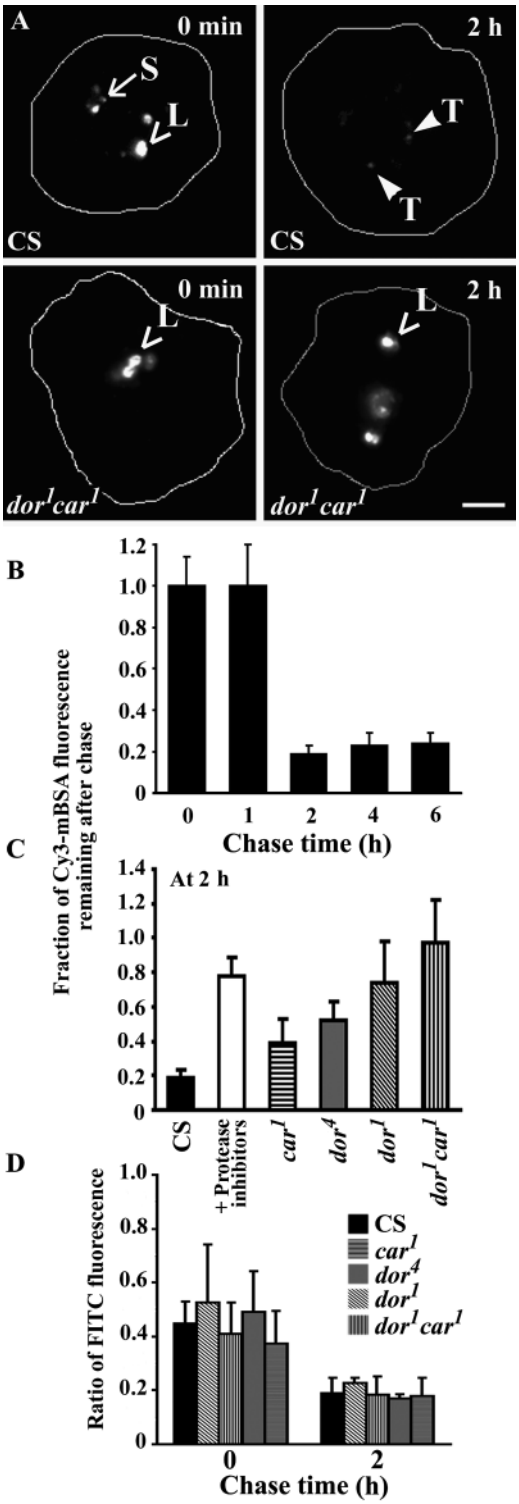

Figure 5. **Endosomal degradation in hemocytes from wild-type and eye color mutant animals.** (A) Hemocytes from wild-type (top) and *dor*^{1}*car*^{1} (bottom) animals were incubated with Cy3-mBSA for 5 min, fixed either immediately (left) or after a 2-h chase (right), and imaged on a wide field microscope. Note the loss in endosomal fluorescence in hemocytes from wild-type compared with *dor*^{1}*car*^{1} after a 2-h chase. (B) Histogram shows quantification of total cell-associated fluorescence of Cy3-mBSA at indicated chase times normalized to cell-associated fluorescence at the 5-min time point. (C) Histogram shows quantification of total cell-associated fluorescence of Cy3-mBSA at 2 h of chase normalized to cell-associated fluorescence at the 5-min time point on treating wild-type cells with a protease inhibitor cocktail or in different alleles as indicated. The differences observed in endosomal degradation between cells from Canton-S and all other alleles were significant ($P < 0.0001$). (D) Histogram shows relative extent of endosomal acidification in cells from indicated mutants, incubated with F-Dex for 5 min, and imaged live, either immediately (0) or after a 2-h chase period (2) on a wide field microscope. Extent of endosomal acidification is expressed as a ratio of FITC fluorescence before neutralization of endosomal pH normalized to FITC fluorescence after neutralization with nigericin. The results shown represent the mean ± SD from two experiments. Bar: 5 μm.

set of compartments. However, in a maturation process the endosomes become the next set of compartments, thus those endosomes accessible to the second pulse would always contain similar levels of the first pulse during the entire chase period. These processes may be distinguished by measuring the ratio of the amount of first pulse to second pulse in colocalized compartments with increasing chase times (Dunn and Maxfield, 1992).

After a 45-min chase period, although most of the endosomes labeled by the first pulse are fusion inaccessible (Fig. 4, C and E), there are a few endosomal structures where the first pulse colocalizes with the second pulse. The ratio of the amount of the first pulse in endosomes marked by the second pulse remains constant throughout the chase period (Fig. 4 F), consistent with a maturation process (Fig. 4 B). This demonstrates that Rab7-positive late endosomes of large multivesicular morphology transform into small dense organelles via a maturation process. After maturation into fusion-inaccessible endosomes, the small sized endosomes finally mix their contents in tubular lysosomes (for example, if cells treated as in Fig. 4 D are further chased for 1 h; data not depicted). Note that these endosomal-morphological transformations are not necessary for the maturation process (Fig. S3, available at http://www.jcb.org/cgi/content/full/jcb.20010166/DC1).

Endosomal degradation in hemocytes from wild-type and eye color mutant alleles of *dor* and *car*

To determine the extent of degradation of endocytosed protein ligands in the endolysosomal system in wild-type (Canton-S strain) cells, Cy3-mBSA was pulsed into cells for 5 min (Fig. 5 A) and chased for different times. Quantification of total cell (Fig. 5 B) and endosome-associated (unpublished data) fluorescence at the end of each chase time showed a dramatic reduction (~80–85%) between 1 and 2 h. At this time, the endocytosed probes are in tubular, Rab7-positive endosomes (Figs. 1–3), indicating this compartment as a major site for endosomal degradation. The reduction in fluorescence is inhibited by a protease-inhibitor cocktail (Fig. 5 C), confirming that loss in fluorescence is a measure of protein degradation in these endosomal compartments.

To determine the effect of mutations in eye color genes, we measured the extent of degradation in cells from wild-type and mutant alleles of *dor* and *car*. Degradation in mutant alleles was significantly reduced compared with wild-type cells (Fig. 5 C); this reduction correlated with severity of the eye color defect (*dor*^{1} > *dor*^{4}). The defect in degradation in the *dor*^{4} mutant cells is rescued by a duplication of the *dor* gene Dp(1:Y)1E (Y*dor*$^{+}$; Narayanan et al., 2000);

the fraction of Cy3-mBSA fluorescence remaining after a 2-h chase of a 5-min pulse with respect to the beginning of the chase in $dor^4/Ydor^+$ is 0.25 ± 0.08 compared with 0.52 ± 0.11 in the dor^4 mutant cells. This is consistent with $Ydor^+$ rescuing the eye color defect in dor^4 mutant animals (unpublished data). These data provide evidence that *dor* is involved in endosomal degradation, consistent with a lack of down-regulation of internalized *wingless* protein in embryos of the null allele, dor^8 (Dubois et al., 2001), and a HRP–Boss fusion protein in dor^8 clone of cells in the *Drosophila* eye (Sevrioukov et al., 1999).

Cells from the only available allele of *car*, car^1 showed a small but significant ($P < 0.0001$) impairment in degradation of Cy3-mBSA after a 2-h chase (Fig. 5 C), suggesting a role for Car in degradation. Although Car associates with Dor in the same protein complex (Sevrioukov et al., 1999), its role in endosomal function is yet to be determined. To test whether *car* is involved with *dor* in endosomal degradation, we used a double mutant of *dor* and *car* (dor^1car^1), which does not survive beyond the prepupal stage as reported previously (Lindsley and Zimm, 1992). The cell culture system that we developed afforded us an opportunity to analyze endosomal trafficking in this mutant combination. Cells from dor^1car^1 showed the most severe defect in endosomal degradation (Fig. 5 A, bottom, and C). There is a small but significant ($P < 0.05$) difference between the degradation defect in dor^1car^1 and dor^1, consistent with a role for both Car and Dor in endosomal degradation.

The impairment of degradation in cells from mutant animals may be due to an acidification defect in mutant cells, causing a perturbation of lysosomal degradation. This possibility is ruled out, since the extent of endosomal acidification in compartments labeled by a 5-min pulse or a subsequent 2-h chase in wild-type and mutant cells are comparable (Fig. 5 D). Another possibility may be due to differences in the extent of internalization of Cy3-mBSA. However, endosomal fluorescence in hemocytes from wild-type and dor^1car^1 is comparable after the 5-min pulse (Fig. 5 A, compare left panels). Thus, the degradation defects observed in the mutant cells are likely to be due to alterations in biogenesis of late endosomes or lysosomes.

Mutant alleles of *dor* and *car* show blockage in morphological transformation at distinct stages of endolysosomal biogenesis but mature with normal kinetics

We next examined the morphology of endosomal compartments accessed by dSR ligands and fluid phase in live hemocytes from dor^4, dor^1, car^1, and dor^1car^1. Following a similar pulse–chase protocol outlined earlier (Fig. 1), we find that the net internalization of probes was not affected in any of the mutants studied (Fig. 5). The probes are delivered to Rab7-positive (unpublished data) large endosomes in all alleles (Fig. 6). Distinct from cells from wild-type (Fig. 1 D) and car^1 animals (Fig. 6 E), the large endosomes in mutant *dor* alleles appear blocked in progression to later stages (Fig.

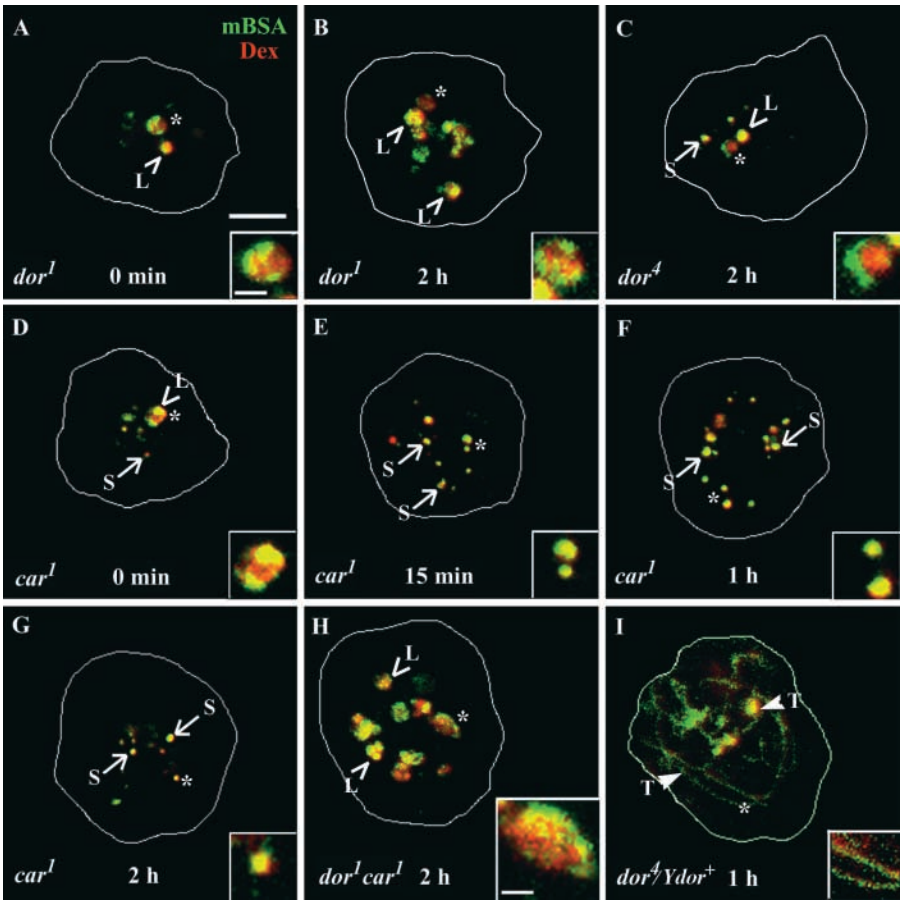

Figure 6. **Hemocytes from mutant alleles of *dor* and *car* show block in distinct stages of endolysosomal traffic.** Hemocytes from indicated mutants were incubated with LR-Dex (red) and A_{488}-mBSA (green) for 5 min, and the morphology of endosomes was visualized by confocal microscopy in living cells either immediately (A and D) or after indicated chase times (B, C, and E–I). In cells from mutant alleles of *dor* and *car*, 5-min endosomes (A and D) contain both probes. Cells from dor^1 and dor^1car^1 do not show endosomal morphological transformation into small sized endosomes even at long chase times (B and H, open arrowheads), whereas endosomes in cells from car^1 undergo rapid morphological transition into small dense organelles (E, arrows) but fail to elaborate tubular structures at longer chase times (F and G). Cells from dor^4 show a marginal endosomal morphological transformation into small sized compartments (arrow) at longer chase times (C, open arrowhead indicates the large compartment). This defect is completely rescued in cells from $dor^4/Ydor^+$ (I, arrowhead, tubular-vesicular compartments). Insets in all panels show magnified view of areas marked by an asterisk. Bars: (shown in A corresponds to A–I) 5 μm; (insets) 1 μm.

6, A and B, *dor*^{1}; C, *dor*^{4}; H, *dor*^{1}*car*^{1}). This defect is completely rescued by overexpression of Dor; in cells from *dor*^{4}/Y*dor*$^{+}$ endosomal progression is similar to wild type (Fig. 6 I). Ultrastructure analysis using HRP as a fluid phase probe showed no difference in the morphology and formation of the MVB and the small dense organelle between *car*^{1} and Canton-S cells (unpublished data). In the cells from the synthetic lethal mutant *dor*^{1}*car*^{1}, after a 2-h chase, many endosomes showed an aberrant distribution of endocytosed probes wherein the dSR ligand is often distributed on the endosomal membrane and the fluid tracer is present in the lumen of exaggerated large sized endosomes (3–4 μm; Fig. 6 H, inset). Cells from *car*^{1} animals exhibited a block in transition of small dense vesicles to tubular-vesicular compartments; even after a chase of 2 h (Fig. 6 G compared with Fig. 1 F) or 4 h (data not depicted) only small vesicular structures are observed.

The distinct effects of mutants of *dor* and *car* on endosomal morphology and progression of endocytosed probes along the pathway described above prompted us to examine the kinetics of loss of fusion accessibility and mechanism of endosomal trafficking in the mutant cells using the protocol established above (Fig. 4). Endosomes in cells from mutant alleles of *dor* and *dor*^{1}*car*^{1}, although incapable of a morphological transition to small dense vesicles, are capable of fusion at early times and normal maturation to fusion inaccessible structures (Fig. S3). Endosomes in cells from the *car*^{1} allele also exhibit wild-type fusion characteristics and mature into fusion-inaccessible small dense structures (Fig. S3). Thus, morphological transformation of endosomes is not essential for normal maturation.

Staining of intracellular organelles with an acidophillic dye in live cells from wild-type and mutant animals is consistent with this interpretation. Lysotracker™ labels all endocytically accessible compartments in wild-type cells, whereas in addition to endocytically accessible organelles, large sized endocytically inaccessible structures are also labeled in *dor*^{1}*car*^{1}. Most of the endocytically inaccessible Lysotracker™-labeled structures in this mutant correspond to phase-lucent vesicles that accumulate inside cells (unpublished data). This suggests that endosomes in mutant cells mature into fusion-inaccessible acidic endosomes, incapable of lateral fusion with each other.

Deep-orange is involved in the delivery of Golgi-derived enzymes to late endosomal compartments

The effects of mutant alleles of *dor* characterized thus far do not provide an explanation for reduced endosomal degradation observed in cells from mutant animals. To determine whether defects in endosomal degradation observed in cells from *dor* alleles are due to alterations in specific trafficking steps, we monitored the delivery of Golgi-derived hydrolases to the endolysosomal system. Cysteine proteinases like cathepsin L are important constituents of the lytic system in lysosomes (Turk et al., 2001; Zwad et al., 2002) and are delivered directly from the Golgi to MVBs and lysosomes in

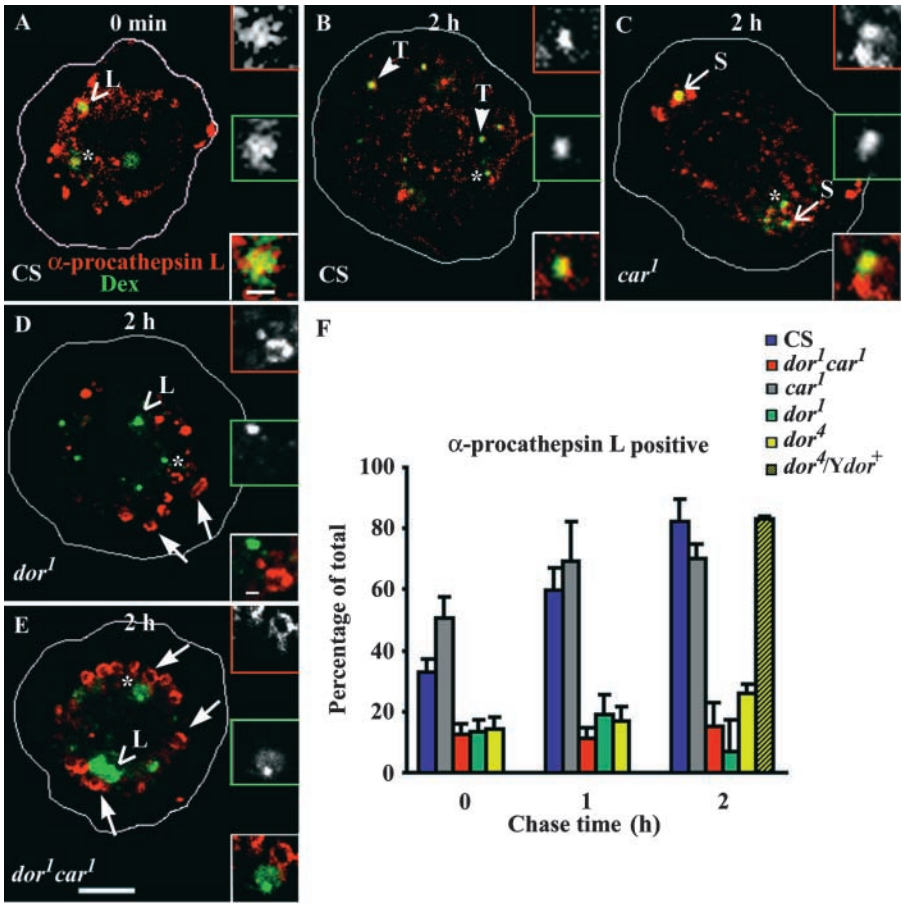

Figure 7. **Mutant alleles of *dor* fail to deliver Golgi-derived hydrolase to endosomes.** Hemocytes from wild-type (A and B), *car*^{1} (C), *dor*^{1} (D), and *dor*^{1}*car*^{1} (E) incubated with F-Dex (green) for 5 (A) or 15 (B–E) min were fixed and immunostained with antiserum against pro–cathepsin L (α-proCathepsin L; red) either immediately (A) or after 2 h (B–E) and imaged on a confocal microscope. Insets in A–E show magnified views of areas marked by an asterisk (α-proCathepsin L, top; F-Dex, middle inset). Note the accumulation of large ring-like organelles containing pro–cathepsin L in the *dor* alleles (D and E, bold arrows). Histogram in F shows the percentage of F-Dex–containing endosomes colocalized with pro–cathepsin L at the indicated chase times in different alleles. Note the complete rescue of defect in fusion of Golgi-derived vesicles with endosomes in hemocytes from *dor*^{4}/Y*dor*$^{+}$. The results represent the mean ± SEM derived from two experiments. Bars: (shown in E corresponds to A–E) 5 μm; (insets) 1 μm.

the pro form where they undergo cleavage to yield the mature proteinase (Turk et al., 2001). To detect the delivery of Golgi cargo we have used antiserum generated against *Sacrophaga peregrina* pro–cathepsin L that cross-reacts with *Drosophila* cathepsin L–like enzyme encoded by *cp1* (Tryselius and Hultmark, 1997) and monitored the time course of intersection of endocytosed F-Dex with this immunoreactivity. At the earliest time monitored (5 min), a fraction (~20%) of large sized F-Dex–containing endosomes is labeled by antiserum against pro–cathepsin L in cells from wild-type (Fig. 7 A, open arrowhead) and car^1 animals (unpublished data). This suggests that at least some of Golgi-derived pro–cathepsin L is delivered to the 5 min, Rab7-positive large sized endosomes. At this time, endosomes in cells from *dor* alleles and dor^1car^1 cells do not show any detectable pro–cathepsin L staining (unpublished data). When a 15-min pulse of F-Dex is chased for longer times in cells from wild-type and car^1 animals an increasing fraction of F-Dex–containing endosomes shows staining for pro–cathepsin L as seen qualitatively in Fig. 7, B and C, and quantitatively in Fig. 7 F. However, in none of the *dor* alleles, is significant pro–cathepsin L staining detected even at late times (Fig. 7, D–F; dor^4, unpublished data). This defect is completely rescued in cells overexpressing Dor ($dor^4/Ydor^+$; Fig. 7 F and Fig. S4, available at http://www.jcb.org/cgi/content/full/jcb.20010166/DC1).

Unlike in wild-type and car^1 cells, wherein pro–cathepsin L is localized to endocytically accessible small and large organelles (Fig. 7, A–C), in all *dor* alleles this protein is present in altogether novel, large ring-like organelles, inaccessible to endosomal probes (Fig. 7, D and E, bold arrows). To check whether these structures represent an altered Golgi from which exit of pro–cathepsin L is blocked, we examined the distribution of a bonafide Golgi marker, lava lamp (Sisson et al., 2000). In all cells, Golgi distribution and morphology, as outlined by lava lamp, is unperturbed (Fig. S5, available at http://www.jcb.org/cgi/content/full/jcb.20010166/DC1) and distinct from the ring-like appearance of pro–cathepsin L structures in the *dor* mutants (Fig. 7, D and E). Furthermore, there is no obvious defect in secretion since dSR-

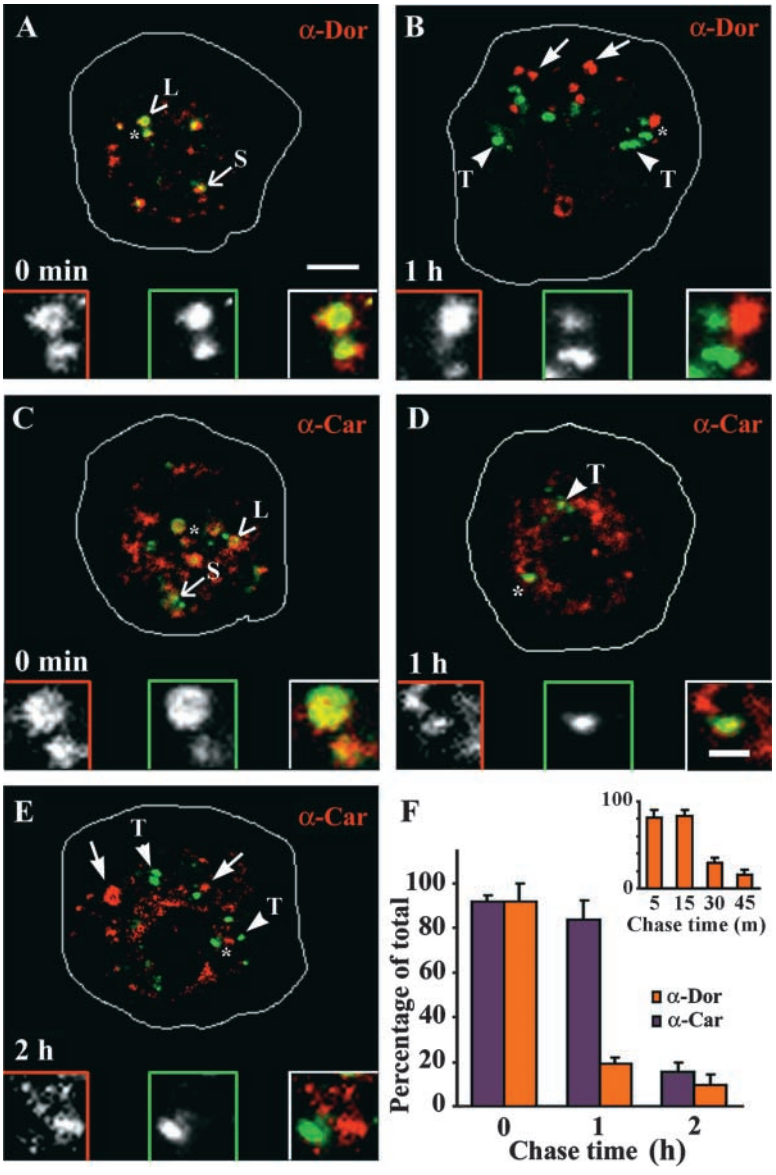

Figure 8. **Localization of Deep-orange and Carnation within the late endolysosomal system in larval hemocytes.** (A–E) Hemocytes incubated with F-Dex (green) for 15 min were fixed and immunostained (red) for Deep-orange (α-Dor) or Carnation (α-Car) either immediately (A and C) or after the indicated chase times (B, D, and E), and imaged on a confocal microscope. Insets show magnified views of the area marked by an asterisk (left, antibody; middle, F-Dex; right, merge). (F) Histogram shows the percentage of F-Dex–containing endosomes colocalized with α-Dor (orange) or α-Car (purple) at the indicated chase times. Histogram in the inset shows percentage of F-Dex–containing endosomes colocalized with α-Dor at shorter chase times. The results shown represent mean ± SEM from three experiments. Bar: (shown in A corresponds to A–E) 5 μm; (insets) 1 μm.

binding capacity at the surface of both mutant and wild-type cells is unaltered (unpublished data). This suggests that both Golgi morphology and secretory function are unperturbed in eye color mutants. The ring-like pro–cathepsin L–containing organelles are likely to represent Golgi-derived vesicles, accumulating in *dor* mutants due to an inhibition of fusion of Golgi vesicles with the late endosomal system. Together, these data suggest that the primary reason for the endosomal degradation defect in mutant alleles of *dor* and in dor^1car^1 is the inability of Golgi-derived (pro–cathepsin L–containing) vesicles to fuse with endocytic compartments, a defect not seen in car^1 cells.

Eye color mutants affect the removal of Dor and Car from Rab7-positive endosomes

To obtain a mechanistic understanding of Dor and Car in biogenesis of endolysosomes, we examined the localization of Dor and Car on different Rab7-positive endosomal compartments in wild-type cells. F-Dex was pulsed and chased into morphologically distinct stages of the endosomal system as before (Fig. 2), and Dor and Car immunoreactivity associated with corresponding compartments was analyzed. Dor is associated with compartments labeled by a 15-min pulse of F-Dex (Fig. 8 A, inset). However, endosomal compartments accessed by a 15-min pulse followed by a 1-h chase are devoid of Dor immunoreactivity (Fig. 8 B, arrowheads). This is similar to observations made in garland cells wherein dextran beads are first seen in Dor-positive compartments and subsequently in Dor-negative compartments (Sevrioukov et al., 1999). Quantitative analysis shows that immediately after a 15-min pulse of F-Dex, 90% of all F-Dex–containing endosomes are α-Dor positive, whereas almost all endosomes accessed after a 1-h chase are devoid of detectable Dor immunoreactivity (Fig. 8 F). In a more detailed temporal analysis, after a pulse of 5 min wherein a majority of endosomes are large sized and Dor positive, a chase of 45-min results in <20% of F-Dex–containing endosomes retaining Dor immunoreactivity on exclusively small sized endosomes observed at this time (Fig. 8 F, inset).

Quantitatively similar to Dor, Car is also associated with all 15-min F-Dex–labeled compartments (Fig. 8, C and F). However, in contrast to Dor, Car is detected on almost all (80%) endosomal compartments after a 1-h chase (Fig. 8, D and F, arrowhead); Car immunoreactivity is lost only after a chase period of 2 h (Fig. 8, E and F), wherein all the endocytosed probe is present in tubular lysosomes (Fig. 2). Together, these data indicate that Dor and Car are associated with the Rab7-positive large MVBs (Fig. S6, available at http://www.jcb.org/cgi/content/full/jcb.20010166/DC1) and small dense endosomes; the small dense endosomes rap-

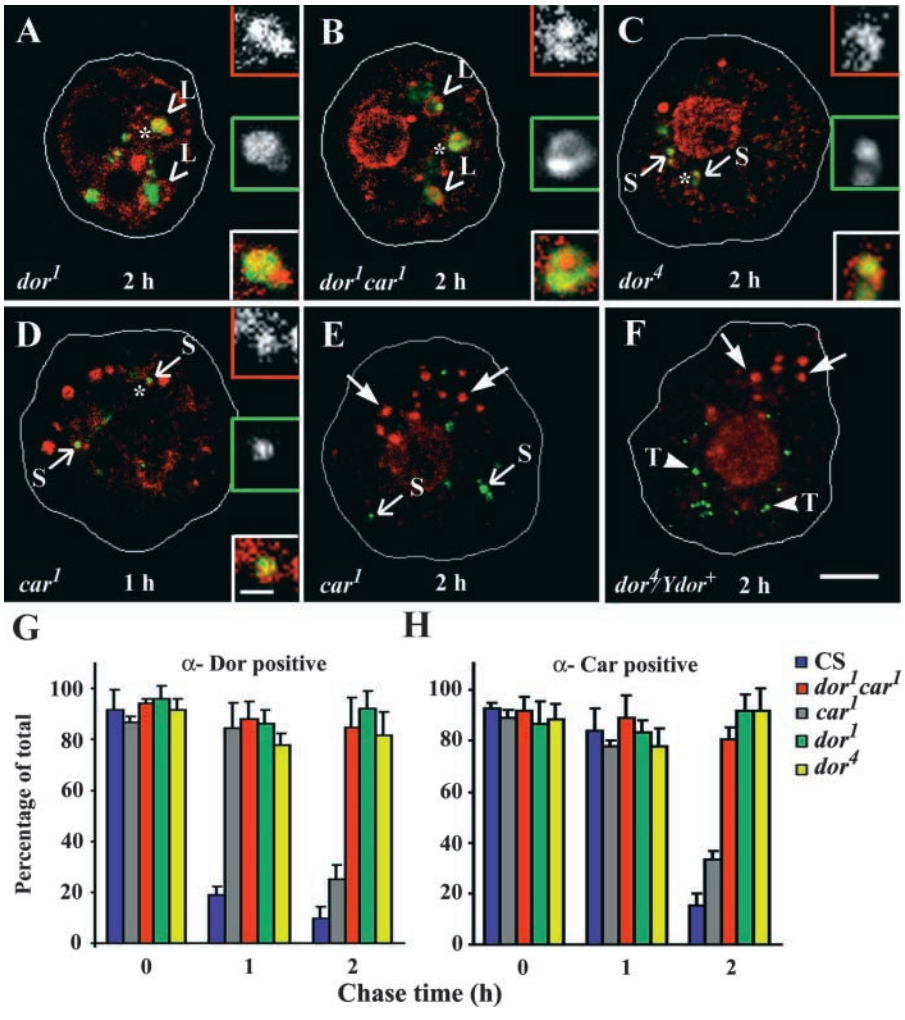

Figure 9. **Eye color mutants affect the removal of Dor and Car from Rab7-positive endosomes.** (A–F) Hemocytes from mutants of *dor* and *car*, synthetic lethal dor^1car^1, and $dor^4/Ydor^+$ were incubated for 15 min with F-Dex (green) and fixed after indicated chase times, immunostained (red) for Deep-orange (α-Dor), and imaged on a confocal microscope. Insets in A–D show magnified view of areas marked by an asterisk (top, antibody; middle, F-Dex; bottom, merge). Bold arrows (E and F) indicate antibody-stained structures lacking endocytic probes. (G and H) Histograms show the percentage of F-Dex–containing endosomes colocalized with α-Dor (G) or α-Car (H) at the indicated chase times in wild-type (blue), dor^1 (green), dor^4 (yellow), dor^1car^1 (red), and car^1 (gray). The results shown represent the mean ± SEM from two experiments. Bars: (shown in F corresponds to A–F) 5 μm; (inset) 1 μm.

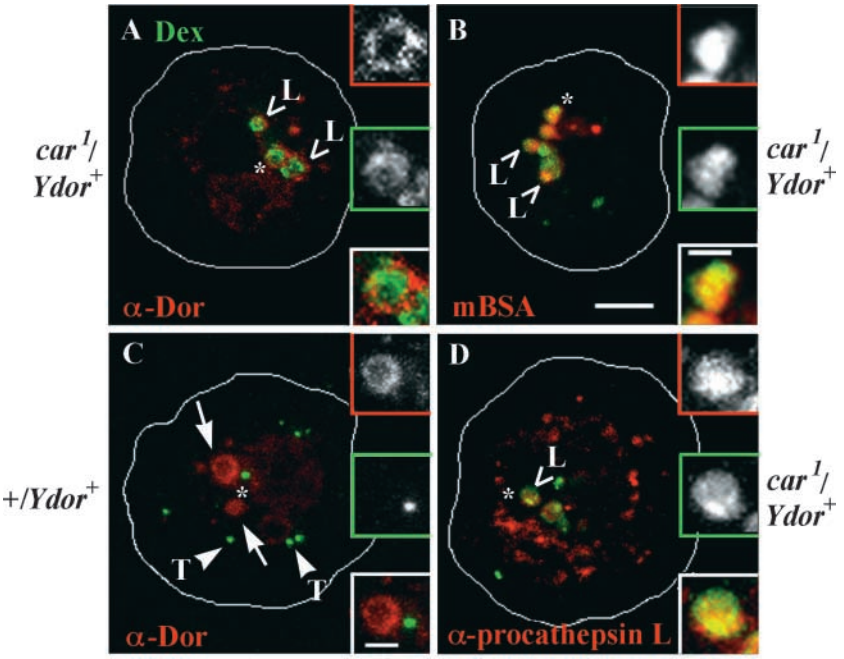

Figure 10. **Endosomal membrane association of Dor and morphological progression in *car[1]/Ydor[+]*.** (A, C, and D) Hemocytes from *car[1]/Ydor[+]* (A and D) and *+/Ydor[+]* (C) were incubated with F-Dex (green) for 15 min followed by a chase of 2 h, fixed and immunostained (red) for Deep-orange (α-Dor; A and C) or pro–cathepsin L (α-proCathepsin L; D), and imaged on a confocal microscope. Insets in A, C, and D show magnified views of areas marked by an asterisk (top, antibody; middle, F-Dex; bottom, merge). Bold arrows indicate antibody-stained structures lacking endocytic probes. (B) Cells from *car[1]/Ydor[+]* were incubated with LR-Dex (red) and A_{488}-mBSA (green) for 5 min, and morphology of endosomes was visualized after a 2-h chase by confocal microscopy in living cells. Insets show magnified views of areas marked by an asterisk (top, Dex; middle, mBSA; bottom, merge). Bars: (shown in B corresponds to A–D) 5 μm; (insets) 1 μm.

idly lose Dor but retain Car reactivity until these structures merge with the tubular lysosomal system. This persistent presence of Car on endosomes that do not have detectable Dor suggests that Car may act independently of Dor in the fusion of small sized endosomes with tubular lysosomes.

In cells from *dor* mutants (including *dor[1]car[1]*), levels of Dor immunostaining are lower than those observed in wild-type hemocytes (unpublished data; Sevrioukov et al., 1999). However, Dor (Fig. 9, A–C and G) and Car (Fig. 9 H) immunoreactivity are persistent on the Rab7-positive large sized endosomes compared with wild-type cells. This defect is completely rescued in cells from *dor[4]/Ydor[+]* animals (Fig. 9 F). These results strongly suggest that mutations in *dor* prevent normal release of Dor and Car proteins from endosomal membranes.

Car regulates Dor association with endosomal membranes and morphological progression of large to small sized endosomes

Endosomes in *car[1]* cells show a wild-type loss of Car immunostaining (Fig. 9 H, gray bars) but are slowed down in the loss of Dor immunoreactivity (Fig. 9, D and E, gray bars, and G), suggesting a function for Car in the removal of Dor from endosomal membranes. To test this role of Car, we examined the kinetics of removal of Dor in cells from animals (*car[1]/Ydor[+]*) that overexpress Dor. Mere overexpression of Dor (in cells from *+/Ydor[+]* animals carrying a duplication of *dor*) shows normal endosomal Dor dissociation kinetics (Fig. 10 C) and endosomal morphological progression (unpublished data). However, overexpression of Dor in cells with mutant Car (*car[1]*) results in a prolonged association (persistent even at 2 h) of Dor on endosomal compartments (Fig. 10 A compared with Fig. 9 E); endosomal morphological transition to small sized compartments is also blocked (Fig. 10 B compared with Fig. 6 G). Furthermore, these endosomes become fusion inaccessible at 30 min, indicating that they mature with wild-type kinetics (unpublished data). These results provide evidence that Car regulates removal of Dor from endosomal membranes; *car[1]* mutation impairs this ability. Arrest of endosomes at the stage of large sized compartments suggests that Car and Dor are required for the morphological transition from large Rab7-positive to small sized endosomes. Endosomal degradation is unchanged with respect to cells from *car[1]* animals (unpublished data) consistent with normal delivery of pro–cathepsin L (Fig. 10 D). Thus, blockage of morphological progression of the endosomes in cells from *car[1]/Ydor[+]* animals is uncoupled from an inhibition of Golgi vesicle delivery (Fig. 10 D) and endosomal degradation.

Discussion

Here we report the characterization of the endolysosomal system in primary cultures of *Drosophila* hemocytes using endogenous markers (Fig. 11, schematic). The ability to visualize endosomal trafficking intermediates using quantitative fluorescence microscopy in living cells from mutant animals provides mechanistic insight into late endosomal maturation. Trafficking between late endosomes and lysosome involves three intermediates with distinct molecular identities (Fig. 11; 5 min, L; 15 min, S; and 45 min, S).

Hemocytes from all mutants of the eye color gene, *dor*, show defects in degradation of the dSR ligand because of the lack of delivery of Golgi-derived hydrolytic enzymes to Rab7-positive MVBs. As observed by immunofluorescence microscopy, aberrant large ring-like structures containing pro–cathepsin L accumulate in cells from mutant *dor* alleles, inaccessible to endocytosed probes. These structures are likely to represent vesicles involved in Golgi to late endosome traffic. This is similar to the vesicles containing Golgi-derived alkaline phosphatase and carboxypeptidase Y that accumulate at the restrictive temperature in a temperature-

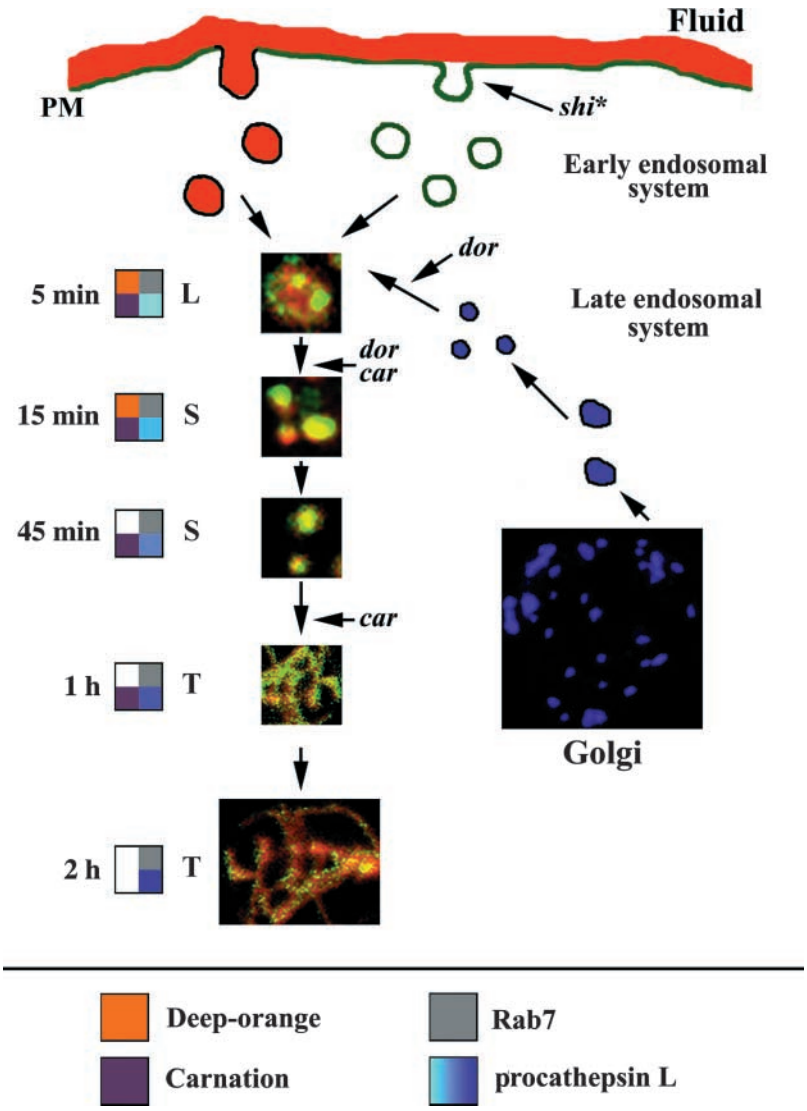

Figure 11. **Schematic of the biogenesis of Rab7-positive endolysosomal system in *Drosophila* hemocytes.** The *Drosophila* scavenger receptor and markers of the fluid phase are internalized by independent endocytic pathways (Guha et al., 2003) and subsequently colocalize in Rab7-positive MVBs in a 5-min pulse of the two probes. These structures are Dor- and Car-positive and are capable of fusion. Multivesicular late endosomes are also accessed by Golgi-derived pro–cathepsin L via a heterotypic fusion reaction. They mature into smaller electron-dense organelles ($t_{1/2}$ ~12 min) and subsequently lose Dor reactivity but remain Car positive. This organelle eventually fuses with a tubular-vesicular Rab7-positive structure; at 2 h the degradation-competent tubular vesicular lysosomes are devoid of Car. Dor (and possibly Car) plays a specific role in endosomal delivery of Golgi-derived cargo (heterotypic fusion). Car regulates Dor membrane association; modulation of Dor governs the morphological progression of the multivesicular bodies to small sized organelles. Car is also involved independent of Dor in fusion of small sized endosomes with tubular lysosomal components. Colored boxes to the left of the model indicate molecular labels of the morphologically distinct endosomes.

sensitive allele of yeast *VPS18* (Rieder and Emr, 1997). These results provide evidence that, similar to Vps18p (Rieder and Emr, 1997), Dor functions in the fusion of Golgi-derived vesicles with the MVB endosomes in a metazoan system.

In contrast to *dor*, only a single mutant allele of another eye color gene, the *Drosophila* homologue of *VPS33*, car^1 (Lindsley and Zimm, 1992), has been characterized. Cells from this mutant background have a small but significant endosomal degradation defect. In this respect, car^1 behaves like a "weak" allele of a mutation in the class C complex genes. Distinct from dor^4 cells that exhibit only a similar defect in endosomal degradation but clearly mislocalize pro–cathepsin L into aberrant structures, pro–cathepsin L is delivered normally to endocytic organelles in cells from car^1. Normal endosomal delivery of pro–cathepsin L in car^1 mutant suggests that there may be a redundant role for Car in this process. In conjunction with genes of the class C complex, *VPS11*, *VPS16*, and *VPS18*, recent studies (Webb et al., 1997; Nichols et al., 1998; Gerrard et al., 2000) have implicated *VPS45* as another *sec1* gene involved in Golgi to endosome traffic in *S. cerevisiae*. It is likely that similar to yeast, in addition to *car*, a *VPS45* homologue may participate in this step (Littleton, 2000). Likely candidates for this gene exist at 85D-E (Lloyd et al., 2000). The reason for a degradation defect may be due to the failure of endosomal contents in car^1 to be well mixed in a large stable pool of degradative enzymes normally found in tubular lysosomes of wild-type cells.

A suggestion for a role for Car in endosomal delivery of Golgi-derived cargo comes from analyses of the endocytic phenotype of cells from the synthetic lethal double mutant $dor^1 car^1$. A small but significant enhancement of the dor^1 endosomal degradation defect and an exaggeration of the aberration of endosomal morphology (compared with the defects observed in dor^1 alone) implicate *car* in the same step; endosomal degradation may be a more sensitive read out of the impairment of delivery of cargo from the Golgi.

Large sized endosomes that accumulate in mutant *dor* alleles and $dor^1 car^1$ mature with normal kinetics into fusion-inaccessible organelles but fail to lose Dor and Car. This suggests that, unlike morphological progression, persistent localization of Dor and Car does not impair maturation. Both the mutations in the *dor* alleles map to the COOH-ter-

minal cysteine-rich RING domain of the protein; *dor*^{4} has a frame-shift mutation, which adds 30 new amino acids, whereas *dor*^{1} has a similar lesion as the *VPS18*^{tsf} allele in terms of a mutation in a RING finger cysteine (Rieder and Emr, 1997). The inability of *dor* mutants to lose Dor immunoreactivity from endosomes may be a consequence of the specific molecular lesion in the RING domain in mutant alleles of *dor*. This is likely to affect the localization dynamics of Car. Car remains persistently localized on the membrane (Fig. 9 H), consistent with a possible physical interaction between Dor and Car (Sevrioukov et al., 1999).

These experiments clearly indicate sequential use of Dor (possibly with other players of the class C complex), first in forming large sized endosomes (fusion between Rab7-positive endosomes and Golgi-derived vesicles) and later in progression to small sized Dor-negative structures. Removal of Dor is implicated in this progression; Dor is retained on the Rab7-positive large endosomes in all *dor* mutants. At the same time, in wild-type and *car*^{1} cells morphological progression of the large sized to small sized endosomes precedes the loss of Dor from the small sized endosomes. This may be explained by a mechanism where Dor function is necessary for this progression and is then followed by inactivation of the membrane-associated Dor leading to its subsequent removal.

Our results suggest that Car is responsible for the inactivation of Dor. This is because in *car*^{1} cells there is delayed endosomal dissociation of Dor from the small sized endosomes, a phenotype that is greatly enhanced by overexpression of Dor (*car*^{1}/Y*dor*$^{+}$ cells; Fig. 10). This overexpression also results in blockage of the morphological transition of the Rab7-positive endosomes (but not its maturation). These observations together suggest that Dor must undergo a Car-dependent modulation necessary for morphological progression to the small sized endosomes, before its removal from the membrane.

Our results implicate Car in a step that is likely to be independent of Dor. First, in wild-type cells, although Dor and Car associate with Rab7-positive MVBs, only Car remains associated with small dense Rab7-positive organelles before fusion with the tubular-vesicular compartments. Second, in the *car*^{1} mutant, Dor-negative and Car-positive small dense endosomal structures formed by maturation of large MVBs that fail to fuse with tubular lysosomes accumulate. This shows that Car remains functionally associated with the endosomal system in the absence of Dor. Consistent with this hypothesis, although Car has been shown to physically interact with Dor, not all membrane-bound Car is in a complex with Dor (Sevrioukov et al., 1999). Furthermore, in yeast Vps33p is obtained in a membrane-associated complex with Vps16p in a deletion strain of *VPS18* (Sato et al., 2000).

Data presented here strongly suggest that although Dor may function similar to *VPS18* in its role in Golgi to endosome traffic, the Sec1p homologue Car may be involved in the Dor-dependent and -independent steps, potentially modulating interaction with endosome stage-specific SNAREs. One of the two point mutations in *car*^{1} (Val to Gly at position 249) is located in the region conserved in all Vps33 family members (Sevrioukov et al., 1999), implicating this region in the regulation of SNARE function. Analyses of the endosomal phenotype of syntaxin 7 mutant fly cells will be necessary to address this question. Finally, the role of Rab7 in the context of this late endosomal pathway needs to be elucidated, since different from yeast, Dor and Car dissect the Rab7-positive endosomal compartments into subsets based on their fusion with either Golgi-derived compartments or with the lysosome.

In conclusion, these studies provide evidence for interplay of Dor and Car in ordering the sequence of endosomal biogenesis. Functional analyses of genes involved in this pathway in a metazoan cell is extremely relevant because these and other studies suggest that the endolysosomal system in higher eukaryotes is likely to be more complex than that present in yeast; some genes involved in cellular functions are present only in higher eukaryotes (Dell'Angelica et al., 2000).

Materials and methods

Materials

All chemicals and media reagents were obtained from Sigma-Aldrich or GIBCO BRL, respectively, unless otherwise specified. Fluorescent dyes for conjugation and Lysotracker™ Red DND-99 were obtained from Molecular Probes. F-Dex and LR-Dex were made as described previously (Sabharanjak et al., 2002). Cy3-mBSA and A_{488}-mBSA were prepared as described (Guha et al., 2003). Secondary antibodies (Jackson ImmunoResearch Laboratories) were conjugated to fluorophores as recommended by the manufacturer.

Fly stocks

All *Drosophila* stocks obtained from the Bloomington Stock Center were grown at 20°C in cornmeal agar bottles. *dor*^{1}*car*^{1} was provided by Mani Ramaswami (University of Arizona, Tucson, AZ). Squash-GAL4 was provided by Dan Kiehart (Duke University, Durham, NC).

Cell culture

Cells from larvae were obtained as described previously (Braun et al., 1998). Briefly, third instar larvae were surface sterilized, and hemolymph was collected by puncturing the integument using dissection forceps into 150 μl of complete medium (CM; Schneider's insect medium supplemented with 10% nonheat inactivated FBS, 1 μg/ml bovine pancreatic insulin, 150 μg/ml penicillin, 250 μg/ml streptomycin, 750 μg/ml glutamine) in 35-mm coverslip-bottom dishes (Mayor et al., 1998). Labeling incubations were performed on adherent hemocytes ~2 h postdissection.

Cell labeling

Adherent hemocytes were washed (three times with medium 1 [Mayor et al., 1998]) before addition of endocytic probes. Fl-mBSA and dextran were used at 800 ng/ml and 1 mg/ml, respectively, in labeling medium (LM; Schneider's insect medium supplemented with 1.5 mg/ml BSA). Hemocytes were incubated with the endocytic probes for the indicated times (pulse period) and washed extensively with medium 1 before further incubation of cells for different intervals of time (chase periods) in CM. Fluorescently labeled mBSA probes were completely competed by incubation of cells with unlabeled mBSA (0.8 mg/ml). Cells were imaged live in imaging medium (IM; medium 1 supplemented with 1 mg/ml BSA and 2 mg/ml D-glucose), or fixed in 2.5% PFA in medium 1 for 20 min before imaging.

Immunofluorescence microscopy

Labeled and fixed cells were permeabilized using 0.4% Igepal for 13 min and incubated in blocking solution (BS; medium 1 with 2 mg/ml BSA), before incubation with primary antiserum. The primary antisera were obtained and used at the indicated dilutions in BS as described in Table I. Cells were incubated with labeled secondary antibodies diluted in BS for 45 min.

Endosomal degradation assays

Cells were incubated with 800 ng/ml Cy3-mBSA for 5 min, washed with medium 1, fixed either immediately or after chase times in CM, and imaged on a wide field microscope. Endosomal degradation was inhibited by using a protease inhibitor cocktail (Set III; Calbiochem). Total fluorescence of cells was determined by marking out a cell outline from the bright field image, and the fluorescence per cell was obtained using Metamorph™ software (Universal Imaging Corp.). Integrated values of cell fluorescence were corrected for background autofluorescence. Extent of degradation

Table I. **Antisera used in this study**

Antigen	Antisera	Dilution	Reference
Deep-orange	Rabbit	1:750	Sevrioukov et al., 1999
Carnation	Rabbit	1:750	Sevrioukov et al., 1999
Hook	Rabbit	1:2,000	Kramer and Phistry, 1996
Pro–cathepsin L	Rabbit	1:100	Tryselius and Hultmark, 1997
Rab7	Rabbit	1:500	Chavrier et al., 1990
Lava lamp	Rabbit	1:5,000	Sisson et al., 2000
Hrs	Guinea pig	1:1,000	Lloyd et al., 2002
LBPA	Mouse monoclonal	1:100	Kobayashi et al., 1998

All of the described antigens in the table are *Drosophila* antigens except for the Rab7 (Canine), pro–cathepsin L (*Sarcophaga perigirina*), and anti-LBPA generated against the Hamster lipid.

was estimated by normalizing the amount of cell-associated fluorescence remaining at the indicated chase time to the amount internalized in 5 min. An experiment consisted of two dishes in which >20 cells per dish were quantified.

Ratiometric pH estimation

To measure endosomal acidification, we used the pH sensitivity of F-Dex (Ohkuma and Poole, 1978). Cells were incubated with F-Dex for 5 min and either imaged immediately or after a 2-h chase. Two images were collected for each field, one before and the other after endosomal pH was neutralized using 10 μM nigericin (Sabharanjak et al., 2002). FITC fluorescence associated with the endosomes per cell before and after addition of nigericin was quantified using Metamorph™ software (Universal Imaging Corp.) and corrected for photobleaching during consecutive exposures. The extent of photobleaching was determined by exposing cells for exactly the same time without any treatment. Ratio of FITC fluorescence associated with the endosomes before addition of nigericin to that after its addition is a measure of the extent of endosomal acidification. Each data point was obtained from >10 cells per allele.

Imaging and image processing

Confocal and wide field imaging was performed exactly as described (Sabharanjak et al., 2002). All images were processed for output purposes using Adobe Photoshop® software.

Quantitative analyses of colocalization

Quantification of colocalization for measuring maturation kinetics was performed as described (Dunn and Maxfield, 1992; Sabharanjak et al., 2002). All processing including determination of colocalization was performed using similar parameters regardless of the type of endocytic tracer used. Colocalization index was calculated as the ratio of the colocalized intensity to the total intensity of the probe in endosomes in each cell. Maximum extent of colocalization obtained by this method is 94% for the colocalization of cointernalized F-Dex and Cy3-mBSA in the same cell. Ratios of fluorophore intensities in individual endosomes were obtained by determining the individual fluorophore intensities in endosome that exhibited colocalization. For the quantification of endocytic probe-containing endosomes colocalized with immunodetected proteins, the total number of endosomes labeled by the endocytic tracer was identified and counted manually using Metamorph™ software (Universal Imaging Corp.). Endosomes positive for the immunodetected protein were recorded and expressed as the percentage of the total number of endosomes. Each experiment consisted of two dishes with >15 cells per dish.

HRP quenching assay

To ascertain lumenal connectivity (Mayor et al., 1998) of optically colocalized Cy3-mBSA and F-Dex in endosomes, HRP was cointernalized as a fluid phase probe along with F-Dex at 1 mg/ml in the presence of 0.5 mg/ml mannan. To prevent the internalization of HRP by mannose receptor expressed on hemocytes, cells were also preincubated with Mannan. To estimate the extent of fusion of two discrete pulses of endocytosed probes, hemocytes were incubated with Cy3-mBSA for 5 min in LM and chased for either 5 or 45 min in CM before a second pulse of 5 min of F-Dex and HRP. HRP-mediated quenching was performed at 4°C for 45 min (Mayor et al., 1998). Fluorescence of Cy3-mBSA and F-Dex was quantified using the Metamorph™ software (Universal Imaging Corp.). The extent of HRP-mediated quenching was expressed as the percentage of Cy3-mBSA fluorescence that was quenched by exposure to H_2O_2. Efficacy of HRP quenching was independently confirmed by ensuring that cointernalized F-Dex fluorescence was completely quenched for each condition.

EM

Hemocytes incubated with 1.5 mg/ml HRP in LM were fixed using 2.5% PFA for 3 min, and HRP enzymatic activity was developed with DAB and 0.003% H_2O_2 diluted in medium 1 at 4°C for 45 min. The cells were washed and postfixed using a mixture of 1.5% gluteraldehyde and 2.5% PFA for 1 h, treated with osmium tetroxide, dehydrated, and embedded in araldite (TAAB). Sections (50–150 nm) were viewed using a Jeol CXII 100 transmission electron microscope. Images were captured on photographic emulsion and scanned at 1,200 dpi for output purposes.

Online supplemental material

Figs. S1–S6 are available at http://www.jcb.org/cgi/content/full/jcb.20010166/DC1. Fig. S1 provides information regarding the specificity of the Rab7 antisera used and the nature of the compartments containg this marker. Fig. S2 shows that Hrs, Deep-orange, Carnation, and Hook are colocalized in the late endolysosomal system in larval hemocytes. Fig. S3 shows that mutant alleles of *dor* and *car* do not affect the maturation kinetics of large sized endosomes. Fig. S4 shows that the block in endosomal delivery of Golgi-derived hydrolase is completely rescued in hemocytes from $dor^4/Ydor^+$. Fig. S5 provides evidence that Golgi morphology is not affected in hemocytes from the eye color mutants. Fig. S6 shows that both Deep-orange and Carnation label GFP-Rab7–positive late endosomes accessed by 5-min pulse of Fl-mBSA.

We thank H. Kramer (University of Texas Southwestern Medical Center, Dallas, TX), S. Natori (RIKEN, Japan), M. Zerial (Max Planck Institute of Molecular Cell Biology and Genetics, Dresden, Germany), and J.C. Sisson and W. Sullivan (University of California, Santa Cruz, CA) for antibodies, M. Ramaswami and R. Narayanan (University of Arizona, Tucson, AZ), M. Gonzalez-Gaitan (Max Planck Institute of Molecular Cell Biology and Genetics), and Dan Kiehart (Duke University, Durham, NC) for fly strains, and C. Sagar and Y. Ramamohan (National Institute of Mental Health and Sciences, Bangalore, India) for EM, and members of the Mayor laboratory for critically reading the manuscript. S. Mayor thanks K. Belur and F.F. Bosphorus for inspiration.

This work was supported by a grant from the Department of Biotechnology, India, and from intramural funds from the National Centre for Biological Sciences. V. Sriram is supported by a Kanwal Rekhi fellowship from the Tata Institute of Fundamental Research endowment fund and Appam. S. Mayor is a Senior Research fellow of the Wellcome Trust.

Submitted: 29 October 2002
Revised: 31 March 2003
Accepted: 2 April 2003

References

Antonin, W., C. Holroyd, D. Fasshauer, S. Pabst, G.F. Von Mollard, and R. Jahn. 2000. A SNARE complex mediating fusion of late endosomes defines conserved properties of SNARE structure and function. *EMBO J.* 19:6453–6464.

Babst, M., G. Odorizzi, E.J. Estepa, and S.D. Emr. 2000. Mammalian tumor susceptibility gene 101 (TSG101) and the yeast homologue, Vps23p, both

function in late endosomal trafficking. *Traffic.* 1:248–258.

Banta, L.M., J.S. Robinson, D.J. Klionsky, and S.D. Emr. 1988. Organelle assembly in yeast: characterization of yeast mutants defective in vacuolar biogenesis and protein sorting. *J. Cell Biol.* 107:1369–1383.

Braun, A., J.A. Hoffmann, and M. Meister. 1998. Analysis of the *Drosophila* host defense in domino mutant larvae, which are devoid of hemocytes. *Proc. Natl. Acad. Sci. USA.* 95:14337–14342.

Bryant, N.J., and T.H. Stevens. 1998. Vacuole biogenesis in *Saccharomyces cerevisiae*: protein transport pathways to the yeast vacuole. *Microbiol. Mol. Biol. Rev.* 62:230–247.

Chavrier, P., R.G. Parton, H.P. Hauri, K. Simons, and M. Zerial. 1990. Localization of low molecular weight GTP binding proteins to exocytic and endocytic compartments. *Cell.* 62:317–329.

Dell'Angelica, E.C., C. Mullins, S. Caplan, and J.S. Bonifacino. 2000. Lysosome-related organelles. *FASEB J.* 14:1265–1278.

Dubois, L., M. Lecourtois, C. Alexandre, E. Hirst, and J.P. Vincent. 2001. Regulated endocytic routing modulates wingless signaling in *Drosophila* embryos. *Cell.* 105:613–624.

Dunn, K.W., and F.R. Maxfield. 1992. Delivery of ligands from sorting endosomes to late endosomes occurs by maturation of sorting endosomes. *J. Cell Biol.* 117:301–310.

Gerrard, S.R., N.J. Bryant, and T.H. Stevens. 2000. VPS21 controls entry of endocytosed and biosynthetic proteins into the yeast prevacuolar compartment. *Mol. Biol. Cell.* 11:613–626.

Glickman, J.N., and S. Kornfeld. 1993. Mannose 6-phosphate-independent targeting of lysosomal enzymes in I-cell disease B lymphoblasts. *J. Cell Biol.* 123: 99–108.

Griffiths, G., B. Hoflack, K. Simons, I. Mellman, and S. Kornfeld. 1988. The mannose 6-phosphate receptor and the biogenesis of lysosomes. *Cell.* 52: 329–341.

Gruenberg, J., and F.R. Maxfield. 1995. Membrane transport in the endocytic pathway. *Curr. Opin. Cell Biol.* 7:552–563.

Gruenberg, J., G. Griffiths, and K.E. Howell. 1989. Characterization of the early endosome and putative endocytic carrier vesicles in vivo and with an assay of vesicle fusion in vitro. *J. Cell Biol.* 108:1301–1316.

Guha, A., V. Sriram, K. S. Krishnan, and S. Mayor. 2003. *shibire* mutations reveal distinct dynamin-independent and dependent endocytic pathways in primary cultures of *Drosophila* hemocytes. *J. Cell Sci*. In press.

Horazdovsky, B.F., D.B. DeWald, and S.D. Emr. 1995. Protein transport to the yeast vacuole. *Curr. Opin. Cell Biol.* 7:544–551.

Knapp, P.E., and J.A. Swanson. 1990. Plasticity of the tubular lysosomal compartment in macrophages. *J. Cell Sci.* 95:433–439.

Kobayashi, T., E. Stang, K.S. Fang, P. de Moerloose, R.G. Parton, and J. Gruenberg. 1998. A lipid associated with the antiphospholipid syndrome regulates endosome structure and function. *Nature.* 392:193–197.

Kramer, H., and M. Phistry. 1996. Mutations in the *Drosophila* hook gene inhibit endocytosis of the boss transmembrane ligand into multivesicular bodies. *J. Cell Biol.* 133:1205–1215.

Krishnan, K.S., S. Chakravarty, S. Rao, V. Raghuram, and M. Ramaswami. 1996. Alleviation of the temperature-sensitive paralytic phenotype of shibire(ts) mutants in *Drosophila* by sub-anesthetic concentrations of carbon dioxide. *J. Neurogenet.* 10:221–238.

Lindsley, D.L., and G.G. Zimm. 1992. The Genome of *Drosophila* melanogaster. Academic Press, Inc., Orlando, FL. 1133 pp.

Littleton, J.T. 2000. A genomic analysis of membrane trafficking and neurotransmitter release in *Drosophila*. *J. Cell Biol.* 150:F77–F82.

Lloyd, T.E., P. Verstreken, E.J. Ostrin, A. Phillippi, O. Lichtarge, and H.J. Bellen. 2000. A genome-wide search for synaptic vesicle cycle proteins in *Drosophila*. *Neuron.* 26:45–50.

Lloyd, T.E., R. Atkinson, M.N. Wu, Y. Zhou, G. Pennetta, and H.J. Bellen. 2002. Hrs regulates endosome membrane invagination and tyrosine kinase receptor signaling in *Drosophila*. *Cell.* 108:261–269.

Lloyd, V., M. Ramaswami, and H. Kramer. 1998. Not just pretty eyes: *Drosophila* eye-colour mutations and lysosomal delivery. *Trends Cell Biol.* 8:257–259.

Luzio, J.P., B.A. Rous, N.A. Bright, P.R. Pryor, B.M. Mullock, and R.C. Piper. 2000. Lysosome-endosome fusion and lysosome biogenesis. *J. Cell Sci.* 113: 1515–1524.

Mayor, S., S. Sabharanjak, and F.R. Maxfield. 1998. Cholesterol-dependent retention of GPI-anchored proteins in endosomes. *EMBO J.* 17:4626–4638.

Mullins, C., and J.S. Bonifacino. 2001. The molecular machinery for lysosome biogenesis. *Bioessays.* 23:333–343.

Narayanan, R., H. Kramer, and M. Ramaswami. 2000. *Drosophila* endosomal proteins hook and deep orange regulate synapse size but not synaptic vesicle recycling. *J. Neurobiol.* 45:105–119.

Nichols, B.J., J.C. Holthuis, and H.R. Pelham. 1998. The Sec1p homologue Vps45p binds to the syntaxin Tlg2p. *Eur. J. Cell Biol.* 77:263–268.

Odorizzi, G., C.R. Cowles, and S.D. Emr. 1998. The AP-3 complex: a coat of many colours. *Trends Cell Biol.* 8:282–288.

Ohkuma, S., and B. Poole. 1978. Fluorescence probe measurement of the intralysosomal pH in living cells and the perturbation of pH by various agents. *Proc. Natl. Acad. Sci. USA.* 75:3327–3331.

Piper, R.C., and J.P. Luzio. 2001. Late endosomes: sorting and partitioning in multivesicular bodies. *Traffic.* 2:612–621.

Rieder, S.E., and S.D. Emr. 1997. A novel RING finger protein complex essential for a late step in protein transport to the yeast vacuole. *Mol. Biol. Cell.* 8:2307–2327.

Robinson, J.S., D.J. Klionsky, L.M. Banta, and S.D. Emr. 1988. Protein sorting in *Saccharomyces cerevisiae*: isolation of mutants defective in the delivery and processing of multiple vacuolar hydrolases. *Mol. Cell. Biol.* 8:4936–4948.

Sabharanjak, S., P. Sharma, R.G. Parton, and S. Mayor. 2002. GPI-anchored proteins are delivered to recycling endosomes via a distinct cdc42-regulated, clathrin-independent pinocytic pathway. *Dev. Cell.* 2:411–423.

Sato, T.K., P. Rehling, M.R. Peterson, and S.D. Emr. 2000. Class C Vps protein complex regulates vacuolar SNARE pairing and is required for vesicle docking/fusion. *Mol. Cell.* 6:661–671.

Sevrioukov, E.A., J.P. He, N. Moghrabi, A. Sunio, and H. Kramer. 1999. A role for the deep orange and carnation eye color genes in lysosomal delivery in *Drosophila*. *Mol Cell.* 4:479–486.

Sisson, J.C., C. Field, R. Ventura, A. Royou, and W. Sullivan. 2000. Lava lamp, a novel peripheral Golgi protein, is required for *Drosophila* melanogaster cellularization. *J. Cell Biol.* 151:905–918.

Spritz, R.A. 1999. Multi-organellar disorders of pigmentation: intracellular traffic jams in mammals, flies and yeast. *Trends Genet.* 15:337–340.

Stoorvogel, W., G.J. Strous, H.J. Geuze, V. Oorschot, and A.L. Schwartz. 1991. Late endosomes derive from early endosomes by maturation. *Cell.* 65:417–427.

Storrie, B., and M. Desjardins. 1996. The biogenesis of lysosomes: is it a kiss and run, continuous fusion and fission process? *Bioessays.* 18:895–903.

Tryselius, Y., and D. Hultmark. 1997. Cysteine proteinase 1 (CP1), a cathepsin L-like enzyme expressed in the *Drosophila* melanogaster haemocyte cell line mbn-2. *Insect Mol. Biol.* 6:173–181.

Turk, V., B. Turk, and D. Turk. 2001. Lysosomal cysteine proteases: facts and opportunities. *EMBO J.* 20:4629–4633.

Webb, G.C., M. Hoedt, L.J. Poole, and E.W. Jones. 1997. Genetic interactions between a pep7 mutation and the PEP12 and VPS45 genes: evidence for a novel SNARE component in transport between the *Saccharomyces cerevisiae* Golgi complex and endosome. *Genetics.* 147:467–478.

Wendland, B., S.D. Emr, and H. Riezman. 1998. Protein traffic in the yeast endocytic and vacuolar protein sorting pathways. *Curr. Opin. Cell Biol.* 10:513–522.

Wickner, W. 2002. Yeast vacuoles and membrane fusion pathways. *EMBO J.* 21: 1241–1247.

Wurmser, A.E., T.K. Sato, and S.D. Emr. 2000. New component of the vacuolar class C-Vps complex couples nucleotide exchange on the Ypt7 GTPase to SNARE-dependent docking and fusion. *J. Cell Biol.* 151:551–562.

Zwad, O., B. Kubler, W. Roth, J.G. Scharf, P. Saftig, C. Peters, and T. Braulke. 2002. Decreased intracellular degradation of insulin-like growth factor binding protein-3 in cathepsin L-deficient fibroblasts. *FEBS Lett.* 510:211–215.